Published in final edited form as:
Adv Funct Mater. 2016 May 10; 26(18): 3154–3163. doi:10.1002/adfm.201505352.

Metal Organic Framework Crystals in Mixed-Matrix Membranes: Impact of the Filler Morphology on the Gas Separation Performance

Anahid Sabetghadam,
Catalysis Engineering-Chemical Engineering Department, Delft University of Technology, Julianalaan, 136, 2628 BL Delft, The Netherlands

Beatriz Seoane[*], **Damla Keskin**,
Catalysis Engineering-Chemical Engineering Department, Delft University of Technology, Julianalaan, 136, 2628 BL Delft, The Netherlands

Nicole Duim, **Tania Rodenas**,
Heterogene Reaktionen, Max-Planck-Institut für Chemische Engergiekonversion, Stifstrasse 34 – 36, D-45470 Mülheim an der Ruhr, Germany

Salman Shahid, and
Catalysis Engineering-Chemical Engineering Department, Delft University of Technology, Julianalaan, 136, 2628 BL Delft, The Netherlands

Sara Sorribas
Chemical and Environmental Engineering Department and Instituto de Nanociencia de Aragón (INA), Universidad de Zaragoza, 50018 Zaragoza, Spain

Clément Le Guillouzer and **Guillaume Clet**
Laboratoire Catalyse et Spectrochimie, ENSICAEN, Université de Caen Basse-Normandie, CNRS, 6 Boulevard Maréchal Juin, 14050 Caen, France

Carlos Tellez,
Chemical and Environmental Engineering Department and Instituto de Nanociencia de Aragón (INA), Universidad de Zaragoza, 50018 Zaragoza, Spain

Prof. Marco Daturi,
Laboratoire Catalyse et Spectrochimie, ENSICAEN, Université de Caen Basse-Normandie, CNRS, 6 Boulevard Maréchal Juin, 14050 Caen, France

Prof. Joaquin Coronas,
Chemical and Environmental Engineering Department and Instituto de Nanociencia de Aragón (INA), Universidad de Zaragoza, 50018 Zaragoza, Spain

Prof. Freek Kapteijn, and
Catalysis Engineering-Chemical Engineering Department, Delft University of Technology, Julianalaan, 136, 2628 BL Delft, The Netherlands

Catalysis Engineering-Chemical Engineering Department, Delft University of Technology, Julianalaan, 136, 2628 BL Delft, The Netherlands j.gascon@tudelft.nl.

Europe PMC Funders Author Manuscripts

Prof. Jorge Gascon*

Abstract

Mixed-matrix membranes (MMMs) comprising NH_2-MIL-53(Al) and Matrimid® or 6FDA-DAM have been investigated. The MOF loading has been varied between 5 and 20 wt%, while NH_2-MIL-53(Al) with three different morphologies: nanoparticles, nanorods and microneedles have been dispersed in Matrimid®. The synthesized membranes have been tested in the separation of CO_2 from CH_4 in an equimolar mixture. At 3 bar and 298 K for 8 wt% MOF loading, incorporation of NH_2-MIL-53(Al) nanoparticles leads to the largest improvement compared to nanorods and microneedles. The incorporation of the best performing filler, *i.e.* NH_2-MIL-53(Al) nanoparticles, to the highly permeable 6FDA-DAM has a larger effect, and the CO_2 permeability increased up to 85 % with slightly lower selectivities for 20 wt% MOF loading. Specifically, these membranes have a permeability of 660 Barrer with CO_2/CH_4 separation factor of 28, leading to a performance very close to the Robeson limit of 2008. Furthermore, a new non-destructive technique based on Raman spectroscopy mapping is introduced to assess the homogeneity of the filler dispersion in the polymer matrix. The MOF contribution can be calculated by modelling the spectra. The determined homogeneity of the MOF filler distribution in the polymer is confirmed by FIB-SEM analysis.

Keywords

Metal-organic frameworks; mixed-matrix membranes; gas separation; NH_2-MIL 53(Al); natural gas and biogas upgrading

1 Introduction

CO_2 is one of the most abundant contaminants in fuel gases such as natural gas and biogas. Its removal by gas upgrading is often necessary, not only to avoid releasing CO_2 to the atmosphere but also to increase fuels heating value and to prevent pipe corrosion.[1] Nowadays, liquid-phase absorption is the most applied technology for CO_2 capture.[2] In particular, the majority of the commercial large-scale absorption processes employ amine-based solutions, such as mono- and triethanolamine or Selexol® (a glycol-based solvent) and Rectisol® (refrigerated methanol) in case of high concentrations of CO_2. .[3] However, this technology presents a large energy penalty, since the need to heat and cool the recirculating fluids requires careful, well-monitored, expensive operating procedures. Furthermore, the degradation of the amine absorbent leads to corrosive mixtures. In this sense, alternative technologies such as selective adsorption or membrane separation may become more attractive.[4]

Membrane technology for gas separation is a promising method in both economic and energy saving terms.[5] In contrast to conventional technologies, such as cryogenic distillation or absorption processes, gas separation membranes do not involve a phase transition, thus being more energy efficient. Furthermore, gas separation membrane units lack of mechanical complexity, are safer and environmentally friendly and have, in general, smaller footprints than other types of plants like amine stripping.[6]

Europe PMC Funders Author Manuscripts

While ceramic or inorganic membranes may have applications in special cases due to their good permselectivity and high thermal and chemical stabilities, the vast majority of commercial gas separation membrane systems are based on polymers because of their easy processability and low cost.[7] However, for different gas pairs, polymeric membranes are known to have a well-established empirical trade-off between permeability and selectivity, which was quantified by Robeson initially in 1991 and then updated in 2008.[8, 9] Therefore, during the last few decades, several approaches have been followed to boost the performance of polymeric membranes. One promising approach is fabricating the so-called mixed matrix membranes (MMMs), which consists of a composite comprising two phases: a polymer matrix and a dispersed phase.[10, 11] The first MMMs were prepared using conventional fillers such as zeolites, carbon molecular sieves and silicas. However, over the last few years new materials have been incorporated, such as carbon nanotubes, clay-type layered silicates, metal organic frameworks (MOFs) or graphene.[11, 12]

Metal-organic frameworks (MOFs) are porous crystalline coordination compounds, extending in one, two or three dimensions, composed of metal atoms or clusters linked by organic ligands.[13] Next to a high surface area and pore volume,[14] their chemical functionality can be fine-tuned by different pre- and post-synthetic approaches; thus, enabling to specifically tailor MOF properties according to the different applications.[15] These properties, together with the flexibility of some structures upon external stimuli,[16] make MOFs ideal for their application in different fields, from gas separation and storage to molecular sensing, catalysis and medical applications.[17, 18] When it comes to MMMs, MOFs have important advantages compared to other fillers.[18, 19] One of the main problems of zeolite-based MMMs is that they commonly suffer from poor polymer-filler compatibility, leading to the formation of defective membranes with non-selective voids at the polymer-filler interface.[20] In this sense, the use of MOFs as fillers might result in a breakthrough in the MMM field, since their partially organic nature provides an enhanced polymer-filler adhesion, preventing the resulting membranes to underperform.[21, 22]

Although MOF-based MMMs have experienced an exponential growth during the last years, few studies have been devoted to the study of the effect of the particle size and morphology on the membrane separation performance. Ge *et al.* compared the performance of MMMs comprising CuBTC with different sizes and poly(2,6-dimethyl-1,4-phenylene oxide) as polymer matrix. Smaller crystals (6 μm) were obtained by post-synthetic ultrasonic treatment and showed a better dispersion and interaction with the polymer than large CuBTC crystals (50 μm), giving rise to an improved separation performance.[23] Furthermore, Nordin *et al.* synthesized MMMs via phase inversion by dispersing ZIF-8 particles of different sizes (100, 300 and 500 nm) in polysulfone. Although the majority of the MMMs showed a decrease in selectivity compared to the bare polysulfone, the incorporation of ZIF-8 with the smallest size led to a 47 % improvement in the CO_2/CH_4 selectivity.[24] However, even though the incorporation of MOF nanoparticles into different polymers has led to outstanding results in the separation of different gas mixtures such as H_2/CO_2,[25] CO_2/CH_4[22, 26] and CO_2/N_2,[27] they are often difficult to disperse, complicating their incorporation within a polymer matrix.[28] In this spirit, we have recently reported the first study on the effect of the particle morphology on the MMMs' microstructure and performance. While bulk CuBDC crystals led to defective membranes

with selectivities lower than those of the bare polymer, the dispersion of CuBDC nanosheets in the polymer gave rise to an enhancement of the CO_2/CH_4 selectivity from 60 for the neat polymer to 80 for 8 wt% MOF loading.[29] This behavior was attributed to the superior occupation and more uniform distribution of the filler in the membrane cross-section if nanosheets are used, showing that in the preparation of MMMs the particle morphology plays a key role.

NH_2-MIL-53(Al) is one of the most studied fillers in the preparation of MMMs together with ZIF-8, HKUST-1 and MIL-53 and it has been dispersed in different polymers, such as PSF,[30–33] 6FDA-based polyimides,[34–36] Matrimid®,[31, 32] poly(4 methyl-1-pentyne) [37] and poly(vinylidene fluoride). This MOF has been reported to possess outstanding selectivities in the separation of CO_2 from equimolar mixtures of CO_2 and CH_4, being a good candidate for the preparation of MMMs.[38] Furthermore, MOFs functionalized with amino groups lead in general to good interaction with different polymer matrices, preventing the formation of voids at the filler-polymer interface, and thus, the fabrication of defective membranes.[35, 38] Herein, we study the effect of the NH_2-MIL-53(Al) crystal morphology on the MMMs microstructure and gas separation performance for the first time. To this end, NH_2-MIL-53(Al) with three different crystal morphologies have been synthesized (nanoparticles, nanorods and microneedles) and used as fillers in the polyimide Matrimid®. The resulting membranes have been tested for CO_2/CH_4 separation and the influence of the MOF loading, crystal morphology and trans-membrane pressure difference on the membrane permeability and selectivity has been assessed. Furthermore, the best performing filler, *i.e.* NH_2-MIL-53(Al) nanoparticles, was also used as dispersed phase in a second polymer matrix, the highly permeable polyimide 6FDA-DAM. With this approach, membranes surpassing the Robeson limit of 1991, and being close to that of 2008, could be obtained upon 20 wt% MOF nanoparticles loading.

2 Results and Discussion

2.1 Characterization of NH_2-MIL-53(Al)

NH_2-MIL-53(Al) crystals with three different morphologies ('nanoparticles' (NP), 'nanorods' (NR) and 'microneedles' (MN)) have been synthesized according to the method reported by Chin *et al.*[39] For comparison purposes, conventional MOF crystals in the submicrometer size range, hereafter referred to as submicron crystals, were also synthesized.[40] In order to examine the size and shape of the different MOFs crystals, TEM images were acquired. The nanoparticles and the nanorods possess the same width (*ca.* 15 nm) but differ in crystal length (Table 1 and Figure 1). While the average length of the nanoparticles is 46 ± 6 nm, the nanorods are 50 % longer with lengths of 67 ± 14 nm. As for the microneedles, the measured aspect ratio was one order of magnitude higher than for the other morphologies with lengths up to 4 ± 1 μm and widths of 80 ± 10 nm.

Figure S1 shows the XRD diffraction patterns obtained for the activated particles with different morphologies. The simulated XRD patterns for the large pore (*lp*) and narrow pore (*np*) NH_2-MIL-53(Al) configurations have also been included for comparison.[41] After activation, the reflections of the nanoparticles, nanorods and microneedles are consistent with a mixture of the *np* and *lp* forms in contrast to the NH_2-MIL-53(Al) submicron crystals,

Europe PMC Funders Author Manuscripts

whose XRD pattern matches with the *np* form. These results are in agreement with previous findings on flexible MOFs, in which the open dried phase is stabilized by crystal downsizing.[42] Indeed, when it comes to high-pressure CO_2 adsorption, the shape of the isotherm is strongly affected by the particle morphology (see Figure S2) and just in the case of the microneedles a pronounced step could be observed.[39] This step has been commonly attributed to flexible MOFs exhibiting 'breathing behavior' or 'gate opening' upon external stimuli. Particularly, in the case of NH_2-MIL-53(Al) this step, taking place at *ca.* 7 bar at 273 K for MOF submicrometer crystals, is related to the breathing of the MOF, which changes from the narrow to the large pore configuration.[43] In the case of NH_2-MIL-53(Al) nanorods and nanoparticles the pressure at which the *lp* configuration starts forming is shifted towards higher pressures compared to the microneedles, the structural transformation taking place over a broader pressure range.[42]

2.2 Characterization and permeation results of NH_2-MIL-53(Al)-based MMMs

2.2.1 NH_2-MIL-53(Al)@Matrimid® MMMs—Characterization

NH_2-MIL-53(Al)@Matrimid® MMMs with two different MOF loadings (8 and 16 wt%) have been prepared with 3 different crystal morphologies (*vide supra*) in order to assess the influence of the morphology of the filler and its loading on membrane structure and performance.

Figure S4 shows the XRD patterns of the NP-NH_2-MIL-53(Al)@Matrimid® MMM synthesized with 16 wt% loading of the nanoparticles along with that of the activated NH_2-MIL-53(Al) nanoparticles and the simulated patterns calculated for the large pore and the narrow pore configurations. The membrane preparation procedure does not affect the crystallinity of the MOF particles in the MMM. Moreover, the intensity of the reflections corresponding to the large pore configuration is higher for the MMM when compared with the activated MOF powder, in line with the results reported by Rodenas *et al.*[32] This behavior has been ascribed to the partial penetration of the polymer chains in the MOF pores during the different steps followed to disperse the filler in the polymer solution in order to prepare a homogeneous casting solution.[32]

In order to assess the filler dispersion on the cross section of the membrane and to evaluate the interaction between the continuous and the dispersed phase, SEM and TEM micrographs were acquired. Figure 2 shows that the distribution of the MOF crystals is homogeneous for the 8 wt% loading MMMs regardless the particle morphology. Furthermore, the TEM micrographs suggest a good interaction between the polymer and the MOF, in agreement with a good affinity between the filler and the polymer not only for the nanoparticles, which exhibit the highest surface to volume ratio, but also for the nanorods.

Gas permeation performance

Figure 3a depicts the CO_2 permeability and the CO_2/CH_4 separation factor of the membranes comprising NH_2-MIL-53(Al) crystals with different morphologies and Matrimid® as a function of the filler loading. The performance of the bare polymer has also been included for comparison.

The gas separation performance of the MMMs is influenced by the morphology of the filler. While the CO_2 permeability of the NP-NH_2-MIL-53(Al)@Matrimid® MMMs increases upon 8 wt% loading, it decreases for both NR-NH_2-MIL-53 and MN-NH_2-MIL-53 (see Figure 3a). We speculate this behavior might be related to a better disruption of the polymer chains by the nanoparticles compared to the nanorods and the microneedles, providing more free volume in the polymeric matrix. As for the selectivity, at 3 bar pressure difference, it remains constant at 8 wt% MOF loading no matter the morphology used, in line with the work of Rodenas *et al.*, who tested NH_2-MIL-53(Al)@Matrimid® MMMs in the separation of CO_2 from an equimolar CO_2/CH_4 at 35 ºC and Δp = 3 bar and observed that the selectivity remained unchanged for MOF loadings up to 15 wt%.[32] This is in agreement with the general trend in MOF-based MMMs, in which the selectivities hardly change upon MOF addition, and with the previous observations of Bae *et al.* for membranes comprising low permeable polymers and highly permeable fillers. Indeed, there is a very large difference between CO_2 permeabilities reported for pure NH_2-MIL-53(Al) membranes (*ca.* 4400 Barrer) and that of the Matrimid® polymer.[22, 38, 44]

When the MOF loading is increased from 8 up to 16 wt%, the permeability decreases at constant or higher separation factors in agreement with reported results on MMMs containing NH_2-MIL-53 as filler and Matrimid® as continuous phase.[32] This behavior is commonly attributed to rigidification of the polymer chains around the filler particles or to the partial blockage of the filler pores.[10] Considering the one-dimensional nature of the pores of the MIL-53 topology both effects would result in lower permeabilities.[45] However, given the fact that low MOF loadings result in higher permeabilities, pore blocking due to polymer penetration into the MOF porosity seems to be rather unlikely. On the other hand, the extent of polymer rigidification increase with increasing MOF loading, with enhancements in the T_g from 324 °C for pure Matrimid® to 327 °C for MMMs containing 16 wt% MOF loading (see Table S2), leading to the observed lower permeabilities at higher filler content. Interestingly, the extent of this rigidification depends on NH_2-MIL-53(Al) crystal morphology, being smaller for nanorods than for nanoparticles (see Table S2).

Finally, the influence of the trans-membrane pressure difference (Δp) on the gas separation performance was studied for 16 wt% NH_2-MIL-53(Al)@Matrimid® MMMs synthesized with the three different crystal morphologies. The studied Δp range lies below the onset of plasticization, which for Matrimid® takes place above 12 bar of CO_2 at 25 ºC.[46] The decrease in CO_2 permeability of bare Matrimid® (Figure 3b) with pressure stems from the decreasing solubility of the polymer (gradual saturation of microvoids), following the predicted behaviour of the dual-mode sorption model.[47, 48]

In contrast, the NH_2 MIL 53-based MMMs show an almost constant permeability at higher pressures, as previously observed in literature and usually attributed to the restricted mobility of the polymer chains in the presence of a filler.[49] Furthermore, the separation factor remains almost constant regardless of the MOF particle morphology.

2.2.2 NH_2-MIL-53(Al)@6FDA-DAM MMMs—Characterization

Since a good match between the permeabilities of the continuous and dispersed phase has been reported to be of utmost importance in the preparation of MOF-based MMMs,[22] another polymer matrix, 6FDA-DAM, with higher CO_2 permeability was used with the best performing filler, *i.e.* NH_2-MIL-53(Al) nanoparticles. In particular, NP-NH_2-MIL-53(Al)@6FDA-DAM MMMs with four different MOF loadings (5, 10, 15 and 20 wt %) have been prepared.

The NP-NH_2-MIL-53(Al)@6FDA-DAM membranes were *ca.* 30 μm thick (see Table S3) according to the measurements performed with a micrometer device, showing no differences at several spots. In order to confirm the thickness of these membranes, laser interference measurements were performed using a Raman spectrometer. Assuming a constant refractive index (n_A = 1.544),[50] the thicknesses determined by both methods for the pure 6FDA-DAM polymer are consistent. By contrast, the values determined for the MMMs were slightly lower than those measured by the micrometer (Table S3). This is likely due to a lowering of the refractive index in the MMM due to the presence of a porous phase.[50] Based on this the refractive indices of the composite membranes can thus be estimated, which turned out to be constant for the investigated NP-NH_2-MIL-53(Al) loadings, and approximately equal to 1.3.

Furthermore, the homogeneity of the filler dispersion in the polymer matrix was evaluated by the Raman spectra of the membranes. Spectra of the individual components and mixed matrix membranes NH_2 MIL 53(Al)@6FDA-DAM are shown in Figure S5. The MMMs did not show any additional absorbance compared to the pure components and the positions of the maxima were not significantly perturbed. Therefore, spectra of the MMMs could be modeled by combining the spectra of the pure components so that the (spectroscopic) contribution of the MOF filler in the membrane could be calculated. In this way comparison of the contributions obtained at different spots on the surface (*ca.* 1 μm^2) yields insight in the homogeneity of the membrane (Figure 4). The analyses carried out at various positions on the NP-NH_2 MIL 53(Al)@6FDA-DAM membranes with different MOF loadings showed a rather good compositional homogeneity. Despite the small size of the spots analyzed, all three membranes showed only a limited variation in the calculated composition. In addition, separate measurements performed on each side of the membranes yielded similar results (Figure 4). The average values correlated with the nominal MOF loading, which confirms that the preparation of these membranes yielded a good dispersion of the MOF filler in the polymer. In order to corroborate these results, FIB-SEM (see Figure S6) micrographs were acquired for the cross sections of NP-NH_2-MIL-53@6FDA-DAM MMMs with 5 and 15 wt % MOF loading before and after FIB milling. In a previous publication we demonstrated the potential of this technique for the in depth characterization of complex composites such as mixed matrix membranes.[21] The images reveal a good spatial (homogeneous) distribution of the filler within the polymer matrix of the 6FDA-DAM-based membranes. Furthermore, the interaction between the continuous and dispersed phase is good and no defects could be observed at the interface. These results are comparable to those reported by Rodenas *et al.*, [21] who calculated void fractions as small as 0.11 % for 25 wt% MMMs comprising NH_2 MIL 53(Al) submicrometer crystals in Matrimid®. Figure S7 shows the gas sorption measurements of CO_2 acquired at 273 K for bare 6FDA-DAM and Matrimid®, 8 wt% NP-NH_2-MIL-53(Al)@6FDA-DAM and 8 wt% NH_2-MIL-53(Al)@Matrimid® MMMs. The gas

adsorption data are sufficient to confirm that the adsorption of Matrimid® was found to be relatively lower than that of 6FDA-DAM, further verifying the high free volume and higher adsorption capacity of the latter. Interestingly, the amount of CO_2 uptake of both Matrimid® and 6FDA-DAM improved by incorporation of NH_2-MIL-53(Al) with different morphologies, what points to a higher solubility of CO_2 in the composite membranes. This higher CO_2 solubility can be attributed to the interaction between CO_2 molecules and the functional groups of the MOF. Moreover, the adsorption capacity is also a measure of the amount of excess free volume in the polymer. It can be speculated that, together with the interaction between CO_2 and the MOF, the addition of NH_2-MIL-53(Al) particles to the polymer matrix could increase the excess free volume of the polymer, which might contribute as well to the higher gas adsorption.

The direct sorption measurement made at 1 bar reflects the dual mode sorption regime, with Langmuir adsorption contributions, from the gas sorption in free volume of polymer and saturation of nanocages of MOFs. At lower pressures, the microvoid space in the polymer matrix is rapidly filled (Langmuir sorption), but this levels off often at higher pressures than studied in this paper, leading to saturation of free empty spaces in the polymer and MMMs. Thus, at lower pressures the influence of solubility is relatively lower than the diffusion contribution in the overall permeation behavior.[48, 49]

Gas permeation performance

Figure 5 depicts the influence of the nanoparticle loading (wt%) in NP-NH_2-MIL-53(Al)@6FDA-DAM MMMs on both the permeability and separation factor. Upon increasing the MOF loading from 0 to 20 wt%, the CO_2 permeability increased from 360 up to 660 Barrer. As mentioned above, the nanoparticles might lead to some disruption of the polymer chains. The enhancement of the free volume, when compared to the bare polyimide, together with the MOF's porosity account for the increased flux through the composite. The enhanced CO_2 permeability can be partly attributed to the higher diffusivity of CO_2 through the MOF particles. CO_2, having a significant quadrupole moment, induces specific interaction with NH_2-MIL-53(Al) promoting its adsorption, while CH_4, lacking a strong interaction with the framework, is adsorbed to a lesser extent. Furthermore, the interaction between the amino and the hydroxyl groups within the NH_2-MIL-53(Al) framework stabilizes its narrow pore configuration, further hampering the diffusion of CH_4 through the MOF channels. The separation factor remains unchanged for MOF loadings between 0 and 10 wt% and slightly decreases with further increase in loading, what could indicate that at such loadings voids are formed at the interface between polymer and MOF. This differs from the constant selectivity reported for NH_2-MIL-53(Al)-based MMMs when PSF,[30] Matrimid®[32] and 6FDA-ODA[34, 36] are used as continuous matrix, but is similar to the published results when other 6FDA-based copolyimides are used instead.[35] Seoane *et al.* showed that depending on the flexibility of the polymers and their functional groups, the affinity between the dispersed and the continuous phase can be modified.[35] In this work, the use of the relatively less flexible monomer DAM might account for defects formed at 15 wt% MOF loading.[51] Moreover, the gas separation performance of the 20 wt% NP-NH_2-MIL-53(Al)@6FDA-DAM MMM was also determined for the separation of CO_2 from N_2 in a 15:85 mixture at 298 and $\Delta p = 1$ bar. Under these conditions both the CO_2/N_2 separation

factor and the CO_2 permeability were slightly increased, from 25 and 715 Barrer for the neat polymer to 26.3 and 737 Barrer upon 20 wt% MOF loading.

Figures 5b and 5c show the performance of bare 6FDA-DAM and NP-NH_2-MIL-53(Al)@6FDA-DAM MMMs at different Δp. The permeability of the pure 6FDA-DAM and the MMMs decreased gradually with increasing Δp, what can be attributed to the saturation of Langmuir sites. Specifically, when the pressure is increased from 3 to 9 bar, the CO_2 permeability drops by 20 % for both the neat 6FDA-DAM membrane and the NP-NH_2-MIL-53(Al)@6FDA-DAM MMM with 20 wt% MOF loading, respectively. In contrast, the CH_4 permeability remained relatively constant, leading to a decrease in selectivity with pressure. Shahid et al.[48] reported that as the pressure is increased the permeability of CO_2 decreases more than that of CH_4 due to the saturation of the favorable Langmuir adsorption sites for CO_2. CH_4 being less affinitive to the neat polymer and MOF suffers relatively less change in its permeability. This behavior is similar as for zeolite membranes for mixtures of weakly and strongly adsorbing components.[52, 53]

Putting the results obtained for the 6FDA-DAM MMMs containing NH_2-MIL-53(Al) nanoparticles in perspective using the customary Robeson plot (see Figure 6), the best results reported in this work surpass the Robeson limit of 1991 and are close to the revisited Robeson limit of 2008.[9] Note that the Robeson plot is constructed for ideal separation factors (based on unary permeation data) at room temperature and that for mixtures these usually deviate in positive or negative direction. In comparison with the most relevant results found in literature for CO_2/CH_4 separation by MOF-based MMMs,[38] our membranes place themselves among the best performing. This is attributed to the good match between the continuous and the dispersed phase, not only in terms in terms of permeability but also in terms of interaction at the interface. A proper choice of the MOF functional groups and particle morphology and aspect ratio is needed to attain better separation performance. These results highlight the importance of crystal engineering of MOFs in the field of mixed matrix membranes and the necessity of synthetic methods able to deliver a high degree of control over MOF formation at all relevant length-scales, from the framework topology and composition to crystal shape and size.

3 Conclusions

Mixed-matrix membranes (MMMs) comprising NH_2-MIL-53(Al) as filler and two different polymer matrices, the polyimides Matrimid® and 6FDA-DAM, have been investigated. For the Matrimid®-based MMMs, NH_2-MIL-53(Al) particles with three different crystal morphologies: nanoparticles, nanorods and microneedles were dispersed in the polymer matrix. The best results were obtained for the NH_2-MIL-53(Al) nanoparticles, which led to an enhancement of the CO_2 permeability at constant selectivities in comparison with the bare Matrimid® membrane and the MMMs containing nanorods and microneedles. Our study reveals that the particle morphology has an impact on the permeation results. Moreover, by using the highly permeable polyimide 6FDA-DAM instead of Matrimid®, the permeability was increased up to 85 % upon NH_2-MIL-53(Al) nanoparticles addition, giving rise to membranes with a performance very close to the 2008 Robeson limit for CO_2/CH_4 separation.

Europe PMC Funders Author Manuscripts

A new non-destructive technique for the characterization (thickness and composition) of the MMMs based on Raman spectroscopy has been introduced. By modeling the polymer and MOF contributions to the Raman spectra of the composite membranes, the filler dispersion in the polymer matrix can be evaluated at different locations. The analysis confirmed the good distribution of the MOF filler in the 6FDA-DAM polymer, in agreement with FIB-SEM analysis.

4 Experimental Section

Synthesis of NH_2-MIL-53(Al) nanoparticles

NH_2-MIL-53(Al) nanoparticles were synthesized under reflux conditions. In a typical synthesis, 1.902 g 2-aminoterephthalic acid (10.50 mmol, Sigma Aldrich, 99 %) was dissolved in 10.5 ml 2 M NaOH aqueous solution at room temperature. Then, 3.935 g $AlCl_3 \cdot 6H_2O$ (16.30 mmol, Sigma Aldrich, ≥99.0 %) was added to a separated vial and both volumes were increased to a total of 7.5 ml by addition of distilled water. The reactants were mixed and treated at reflux temperature for 3 days without stirring. The resulting yellow powders were filtered under vacuum and activated to remove organic species trapped within the pores with N,N-dimethylformamide (DMF, Sigma Aldrich, > 99.8 %) at 403 K, and subsequently with methanol under reflux, overnight. Finally, the powder was thoroughly washed twice with ethanol and dried at 373 K under vacuum.

Synthesis of NH_2-MIL-53(Al) nanorods

NH_2-MIL-53(Al) nanorods were synthesized according to the method reported by Chin *et al.* [39] Two different solutions were prepared separately in 15.6 ml deionized water: 0.589 g 2-aminoterephthalic acid (3.25 mmol, Sigma Aldrich, 99 %) together with 0.898 g sodium acetate (10.95 mmol, Sigma Aldrich, 99 %), giving rise to a pale yellow solution, and 0.821 g $Al(NO_3)_3 \cdot 9H_2O$ (2.20 mmol, Fluka, 98 %). Both solutions were mixed in a Teflon®-lined autoclave and the synthesis solution was treated at 393 K for 3 days in an oven under static conditions. The resulting powder was washed with acetone and centrifuged at 6000 rpm for 10 min. To efficiently eliminate the remaining linker occluded in the pores of the MOF, the solid was consecutively re-suspended in 30 ml N,N-dimethylformamide (DMF) and 30 ml methanol and treated at 403 K and 363 K overnight, respectively. Finally, the powder was centrifuged at 6000 rpm for 10 min, thoroughly washed twice with ethanol and dried at 353 K under vacuum.

Synthesis of NH_2-MIL-53(Al) microneedles

To synthesize NH_2-MIL-53(Al) microneedles the method reported by Chin *et al.*[39] was followed. Two different solutions were prepared in 15 ml DMF: 0.565 g 2-aminoterephthalic acid (3.12 mmol, Sigma Aldrich, 99 %) together with 3.783 g acetic acid (63 mmol, Sigma Aldrich, 99 %), giving rise to a pale yellow solution, and 0.788 g $Al(NO_3)_3 \cdot 9H_2O$. Both solutions were mixed in a Teflon®-lined autoclave. The synthesis solution was then treated at 393 K for 3 days in an oven under static conditions. The washing and drying procedure was the same as for the nanorods.

6FDA-DAM polyimide synthesis

The monomers used for the polyimide synthesis – 4,4'-(hexafluoroisopropylidene) diphthalic anhydride (6FDA, Sigma Aldrich, 99 %) and 2,4,6 trimethyl-*m*-phenylenediamine (DAM, Sigma Aldrich, 96 %) – were purified by sublimation prior to their use. Besides, dimethylacetamide (DMAc, Acros Organics, 99.5 %), acetic anhydride and triethylamine (TEA, Sigma Aldrich, > 99 %) were used as received.

To synthesize the polyimide, a two-step procedure was followed. In the first step the diamine (1.5022 g, 10 mmol) was dissolved in DMAc (8 mL) in a moisture free flask under Ar atmosphere and 6FDA (4.4424 g, 10 mmol) was added in small portions together with another 8 mL of DMAc. Then, the mixture was stirred overnight and polyamic acid (PAA) was formed. In the second step PAA was chemically imidized using an equimolar, three-fold excess (based on the total amount of diamine monomers) of triethylamine/acetic anhydride mixture, and the mixture was heated up to 393 K for 30 min. After cooling, the polymer was precipitated in a 1:1 volume mixture of ethanol and distilled water, milled and washed with ethanol. The molecular weight of the synthesized polymer as measured by gel permeation chromatography was Mw = 123000 g/mol and Mn = 68000 g/mol.

Preparation of mixed-matrix membranes (MMMs)

Two different polyimides were used as polymeric matrices in the MMMs: Matrimid® 5218 (supplied by Huntsman Advanced Materials, Mw ≈ 80000 g/mol and Mn ≈ 11000 g/mol) and 6FDA-DAM (*vide supra*). Prior to the membranes synthesis, the polymers were degassed overnight at 453 K under vacuum in order to remove the adsorbed moisture. To prepare the MMMs, 0.4 g dried polymer was dissolved in 2.5 ml tetrahydrofuran (THF) and, in the case of 6FDA-DAM-based MMMs, the polymer solution was filtered through a syringe filter (PTFE membrane, 0.45 μm pore size). Then, MOF crystals were suspended in 1.55 ml THF under ultrasonication for 60 min. To this suspension, 10 % of the dissolved polymer amount was added and the suspension further stirred for 4 h (priming). After that, the rest of the polymer solution was added to the MOF suspension and stirred overnight. The solvent/filler-polymer weight ratio was of 90/10 in all cases. The MOF content in this synthesis suspension was adjusted to achieve final desired MOF loadings in the resulting membranes. For comparison, membranes based on the neat polymers were also prepared following an identical procedure, but without MOF incorporation. The casting suspension was poured on the glass slide of a Doctor Blade setup to cast the membrane with 75 μm thickness. After casting, the membranes were covered with a top-drilled box (30.5 cm length x 15.5 cm height x 23.0 cm width) and dried overnight under THF-saturated atmosphere at room temperature (RT) by natural convective evaporation. Finally, membranes were treated under vacuum at 453 K during 24 h.

Characterization methods

XRD patterns of the prepared MOF powder and the membranes were recorded in a Bruker-D8 Advance diffractometer using Co-K_α radiation (λ = 1.78897Å). The 2θ range of 5–50° was scanned using a step size of 0.02° and a scan speed of 0.2 s per step in a continuous scanning mode.

High-pressure adsorption isotherms of CO_2 were measured for MOF powder samples with different types of morphologies. The CO_2 isotherms were determined using the volumetric technique with an apparatus from BEL Japan (Belsorp HP) at 273 K. Around 0.2 g NH_2-MIL-53(Al) nanoparticles was placed in the sample container. Before the measurement, the adsorbent was pretreated by increasing the temperature to 423 K at a rate of 10 K/min under N_2 flow and maintaining the temperature for 2 h. Furthermore, CO_2 isotherms were acquired for neat and mixed-matrix membranes. The different samples were first degassed under vacuum at 200 °C for 16 h and then analyze with a Tristar II 3020 (Micromeritics) apparatus using high purity CO_2 (Linde, 99.995 %).

For the TEM analysis the MOF powder samples were prepared by applying a few drops of MOF suspensions in ethanol on a carbon coated copper grid and dried. TEM analyses were carried out in JEOL JEM-2010 microscope operated at 200 keV. This microscope has an X-ray OXFORD detector, INCA energy TEM 100 model for microanalysis (EDS) and a bottom-mounted GATAN ORIUS SC600 imaging camera. Micrograph acquisition was performed with GATAN DigitalMicrograph 1.80.70 software. As for the MMMs, a portion of the membrane was embedded in an EpofixTM cold-setting embedding resin (in volume proportion, 15 parts of embedding resin and 2 parts of hardener) and cured for 24 h at room temperature. Afterwards, slices of 100 nm thickness were cut using a Leica EMUC7 ultramicrotome and placed on carbon copper. Membrane cross-sectional images were taken by transmission electron microscopy (TEM), with a Tecnai T20 operating at 200 kV.

Prior to the FIB-SEM analyses, the membranes were prepared by freeze-fracturing after immersion in liquid N_2 and coated with platinum. A trench was milled in the specimen by accelerating concentrated gallium ions (30 kV, 0.75 nA) using a Dual Beam 3 Nova 200 FIB. Several cross-sections of 15 x 10 μm^2 were exposed by FIB milling and individual SEM images of the exposed surfaces were recorded.

DSC measurements were performed using Perkin Elmer DSC 7 equipment to estimate glass transition temperature of the neat and MMMs. The scanning range was 25 – 425 °C at a heating rate of 10 °C/min under nitrogen atmosphere. Two consecutive runs were performed. A first DSC cycle was carried out to remove thermal history and to remove adsorbed water from the samples. After cooling, a second cycle was performed following the same procedure. The glass transition temperature (T_g) value was taken from the middle point of the slope transition in the DSC curve.

Membrane thickness (μm), l, was determined using a digital micrometer Mitutoyo, with an accuracy of 1 μm. The measurement was performed at least at 10 different locations within each membrane and then averaged.

Raman experiments were conducted on the membranes in a Jobin Yvon Labram 300 confocal microscope equipped with a laser at 633 nm and a 1800 lines/mm grating. Alternatively, the spectrometer was also used to monitor the interferences of the laser light when passing through the membranes. From Equation 1, and by comparison with the measured membrane thickness (*vide supra*), either the membrane thickness or the refractive index of the material was calculated.

$$l = \frac{\Delta_m}{2 \cdot n_A \cdot (\sigma_2 - \sigma_1)} \quad \text{Equation (1)}$$

Where Δm is the number of periods between the wavenumbers σ_1 and σ_2, and n_A is the refractive index of the material.

The homogeneity of the membranes for the dispersion of the filler in the polymer was estimated from the Raman intensities in the membrane compared to the spectra of the pure components. For this, at least 15 measurements were done at several spots (*ca.* 1 μm^2) on both sides of the membrane surface. All the spectra of the MMMs were then modeled by combining the same reference spectra of the pure MOF and polymer. The spectroscopic contribution of the MOF filler in the membrane was calculated using the spectrometer's software LabSpec 5. The numerical value of the calculated ratio was found to vary if different reference spectra were used for the modeling. However, for each set of common reference spectra, a similar evolution of the average ratios was obtained with the MOF loading.

Gas permeation experiments

Round membrane sheets with an area of 4.15 cm^2 were cut from the casted films, placed on a macroporous support 316L with 20 μm nominal pore size and mounted in a flange between Viton® O-rings. This flange fit in a permeation module was placed inside an oven using the permeation setup described elsewhere.[30] The CO_2/CH_4 separation measurements were carried out in a home-made setup employing a 1:1 flow mixture of CO_2 and CH_4 (50 $ml \cdot min^{-1}$ of CO_2 and 50 $ml \cdot min^{-1}$ of CH_4) as feed. Helium (3.3 $ml \cdot min^{-1}$) was used as sweep gas for the permeate stream (atmospheric), while the trans-membrane pressure was adjusted in the range of 3-9 bar using a back-pressure controller at the retentate side. All the reported gas separation results were determined after at least 10 h of operation once the steady performance had been reached at each set of experimental conditions during the gas permeation experiments.[21] The temperature in the permeation module was 298 K. An on-line gas chromatograph (Interscience Compact GC) equipped with a packed Carboxen 1010 PLOT (30 m x 0.32 mm) column and TCD and FID detectors was used to periodically analyze the permeate stream.

Each membrane was fabricated and measured at least two times to ensure the reproducibility of the results. In all cases, gas separation performance was evaluated after ensuring steady operation.

Gas separation performance was defined by the separation factor (α) and the gas permeability (P) of the individual components. The permeability for the component i (P_i) was calculated as follows (Equation 2):

$$P_i = \frac{F_i \cdot l}{\Delta p_i \cdot A} \quad \text{Equation (2)}$$

where F_i denotes the molar flow rate of i-compound, l is the thickness of the membrane, Δp_i is the partial pressure difference of i across the membrane and A is the membrane area.

The SI unit for the permeability is $mol \cdot s^{-1} \cdot m \cdot m^{-2} \cdot Pa^{-1}$. However, gas permeabilities are reported in the widely used non-SI unit Barrer, where 1 Barrer = 3.35×10^{-16} $mol \cdot s^{-1} \cdot m \cdot m^{-2} \cdot Pa^{-1}$.

The separation factor or mixed gas selectivity (α) was calculated as the ratio of the permeability of the more permeable compound, CO_2, to the permeability of the less permeable compound, CH_4 (Equation 3).

$$\alpha = \frac{P_{CO2}}{P_{CH4}} \quad \text{Equation (3)}$$

Supporting Information

Refer to Web version on PubMed Central for supplementary material.

Acknowledgements

A. Sabetghadam and D. Keskin contributed equally to this work. The authors acknowledge the financial support of the European Research Council under the European Union's Seventh Framework Programme (FP/2007-2013), M^4CO_2 project and ERC Grant Agreement no. 335746, CrystEng-MOF-MMM and the Laboratorio de Microscopías Avanzadas at the Instituto de Nanociencia de Aragón for offering access to their instruments and expertise.

References

[1]. Andriani D, Wresta A, Atmaja TD, Saepudin A. Appl Biochem Biotech. 2014; 172:1909.

[2]. a) Niesner J, Jecha D, Stehlik P. Chem Eng Trans. 2013; 35:517.b) Figueroa JD, Fout T, Plasynski S, McIlvried H, Srivastava RD. Int J Greenh Gas Control. 2008; 2:9.

[3]. Karadas F, Atilhan M, Aparicio S. Energy Fuels. 2010; 24:5817.

[4]. Tagliabue M, Farrusseng D, Valencia S, Aguado S, Ravon U, Rizzo C, Corma A, Mirodatos C. Chem Eng J. 2009; 155:553.

[5]. Bernardo P, Drioli E, Golemme G. Ind Eng Chem Res. 2009; 48:4638.

[6]. He X, Hägg: MB. Membranes. 2012; 2:706. [PubMed: 24958426]

[7]. Gascon J, Kapteijn F, Zornoza B, Sebastian V, Casado C, Coronas J. Chem Mater. 2012; 24:2829.

[8]. Robeson LM. J Membr Sci. 1991; 62:165.

[9]. Robeson LM. J Membr Sci. 2008; 320:390.

[10]. Chung TS, Jiang LY, Li Y, Kulprathipanja S. Prog Polym Sci. 2007; 32:483.

[11]. Dong GX, Li HY, Chen VK. J Mater Chem A. 2013; 1:4610.

[12]. Goh PS, Ismail AF, Sanip SM, Ng BC, Aziz M. Sep Purif Technol. 2011; 81:243.

[13]. a) Batten SR, Champness NR, Chen XM, Garcia-Martinez J, Kitagawa S, Ohrstrom L, O'Keeffe M, Suh MP, Reedijk J. Pure Appl Chem. 2013; 85:1715.b) Li H, Eddaoudi M, O'Keeffe M, Yaghi OM. Nature. 1999; 402:276.

[14]. Farha OK, Eryazici I, Jeong NC, Hauser BG, Wilmer CE, Sarjeant AA, Snurr RQ, Nguyen ST, Yazaydin AÖ, Hupp JT. Am Chem Soc. 2012; 134:15016.

[15]. a) Eddaoudi M, Kim J, Rosi N, Vodak D, Wachter J, O'Keeffe M, Yaghi OM. Science. 2002; 295:469. [PubMed: 11799235] b) Wang ZQ, Cohen SM. Chem Soc Rev. 2009; 38:1315. [PubMed: 19384440]

[16]. a) Ferey G, Serre C. Soc Rev. 2009; 38:1380.b Seoane B, Sorribas S, Mayoral Á, Téllez C, Coronas J. Microporous Mesoporous Mater. 2015; 203:17.

[17]. a) Gascon J, Corma A, Kapteijn F, Llabrés i Xamena FX. ACS Catal. 2013; 4:361.b) Liu B. J Mater Chem. 2012; 22:10094.c) Kreno LE, Leong K, Farha OK, Allendorf M, Van Duyne RP, Hupp JT. Chem Rev. 2012; 112:1105. [PubMed: 22070233]

[18]. Shah M, McCarthy MC, Sachdeva S, Lee AK, Jeong HK. Ind Eng Chem Res. 2012; 51:2179.

[19]. a) Zornoza B, Tellez C, Coronas J, Gascon J, Kapteijn F. Microporous Mesoporous Mater. 2013; 166:67.b) Jeazet HBT, Staudt C, Janiak C. Dalton Trans. 2012; 41:14003. [PubMed: 23070078] c) Erucar I, Yilmaz G, Keskin S. Chem Asian J. 2013; 8:1692. [PubMed: 23526663]

[20]. Moore TT, Koros WJ. J Mol Struct. 2005; 739:87.

[21]. Rodenas T, van Dalen M, Garcia-Perez E, Serra-Crespo P, Zornoza B, Kapteijn F, Gascon J. Funct Mater. 2014; 24:249.

[22]. Bae TH, Lee JS, Qiu WL, Koros WJ, Jones CW, Nair S. Angew Chem. 2010; 122:10059.Angew Chem Int Ed. 2010; 49:9863.

[23]. Ge L, Zhou W, Rudolph V, Zhu ZH. J Mater Chem A. 2013; 1:6350.

[24]. Nordin NAHM, Ismail AF, Mustafa A, Murali RS, Matsuura T. RSC Adv. 2014; 4:52530.

[25]. a) Yang T, Chung TS. Int J Hydrogen Energy. 2013; 38:229.b) Cao LJ, Tao K, Huang AS, Kong CL, Chen L. Chem Commun. 2013; 49:8513.c) Wijenayake SN, Panapitiya NP, Versteeg SH, Nguyen CN, Goel S, Balkus KJ, Musselman IH, Ferraris JP. Ind Eng Chem Res. 2013; 52:6991.d) Yang TX, Chung TS. J Mater Chem A. 2013; 1:6081.

[26]. a) Bushell AF, Attfield MP, Mason CR, Budd PM, Yampolskii Y, Starannikova L, Rebrov A, Bazzarelli F, Bernardo P, Jansen JC, Lanc M, et al. J Membr Sci. 2013; 427:48.b) Hsieh JO, Balkus KJ, Ferraris JP, Musselman IH. Microporous Mesoporous Mater. 2014; 196:165.

[27]. a) Li T, Pan YC, Peinemann KV, Lai ZP. J Membr Sci. 2013; 425:235.b) Nafisi V, Hagg MB. J Membr Sci. 2014; 459:244.

[28]. Seoane B, Sebastian V, Tellez C, Coronas J. CrystEngComm. 2013; 15:9483.

[29]. Rodenas T, Luz I, Prieto G, Seoane B, Miro H, Corma A, Kapteijn F, Xamena FXLI, Gascon J. Nat Mater. 2015; 14:48. [PubMed: 25362353]

[30]. Zornoza B, Martinez-Joaristi A, Serra-Crespo P, Tellez C, Coronas J, Gascon J, Kapteijn F. Chem Commun. 2011; 47:9522.

[31]. Valero M, Zornoza B, Tellez C, Coronas J. Microporous Mesoporous Mater. 2014; 192:23.

[32]. Rodenas T, van Dalen M, Serra-Crespo P, Kapteijn F, Gascon J. Microporous Mesoporous Mater. 2014; 192:35.

[33]. Burmann P, Zornoza B, Tellez C, Coronas J. Chem Eng Sci. 2014; 107:66.

[34]. Chen XY, Vinh-Thang H, Rodrigue D, Kaliaguine S. Ind Eng Chem Res. 2012; 51:6895.

[35]. Seoane B, Tellez C, Coronas J, Staudt C. Sep Purif Technol. 2013; 111:72.

[36]. Chen XY, Hoang VT, Rodrigue D, Kaliaguine S. RSC Adv. 2013; 3:24266.

[37]. Abedini R, Omidkhah M, Dorosti F. RSC Adv. 2014; 4:36522.

[38]. Seoane B, Coronas J, Gascon I, Benavides ME, Karvan O, Caro J, Kapteijn F, Gascon J. Chem Soc Rev. 2015; 44:2421. [PubMed: 25692487]

[39]. Chin JM, Chen EY, Menon AG, Tan HY, Hor ATS, Schreyer MK, Xu JW. CrystEngComm. 2013; 15:654.

[40]. Ahnfeldt T, Gunzelmann D, Loiseau T, Hirsemann D, Senker J, Ferey G, Stock N. Inorg Chem. 2009; 48:3057. [PubMed: 19245258]

[41]. Couck S, Gobechiya E, Kirschhock CEA, Serra-Crespo P, Juan-Alcaniz J, Joaristi AM, Stavitski E, Gascon J, Kapteijn F, Baron GV, Denayer JFM. ChemSusChem. 2012; 5:740. [PubMed: 22378615]

[42]. Sakata Y, Furukawa S, Kondo M, Hirai K, Horike N, Takashima Y, Uehara H, Louvain N, Meilikhov M, Tsuruoka T, Isoda S, et al. Science. 2013; 339:193. [PubMed: 23307740]

[43]. Serra-Crespo P, Gobechiya E, Ramos-Fernandez EV, Juan-Alcaniz J, Martinez-Joaristi A, Stavitski E, Kirschhock CEA, Martens JA, Kapteijn F, Gascon J. Langmuir. 2012; 28:12916. [PubMed: 22891682]

[44]. Zhang F, Zou XQ, Gao X, Fan SJ, Sun FX, Ren H, Zhu GS. Adv Funct Mater. 2012; 22:3583.
[45]. Ren HQ, Jin JY, Hu J, Liu HL. Ind Eng Chem Res. 2012; 51:10156.
[46]. Bos A, Punt IGM, Wessling M, Strathmann H. J Membr Sci. 1999; 155:67.
[47]. a) Paul DR. Ber Bunsen-Ges Phys Chem. 1979; 83:294.b) Stannett V. J Membr Sci. 1978; 3:97.
[48]. Shahid S, Nijmeijer K. J Membr Sci. 2014; 459:33.
[49]. Shahid S, Nijmeijer K. J Membr Sci. 2014; 470:166.
[50]. Kim JH, Koros WJ, Paul DR. Polymer. 2006; 47:3104.
[51]. Velioglu S, Ahunbay MG, Tantekin-Ersolmaz SB. J Membr Sci. 2012; 417:217.
[52]. Zhu W, Hrabanek P, Gora L, Kapteijn F, Moulijn JA. Ind Eng Chem Res. 2006; 45:767.
[53]. Voss H, Diefenbacher A, Schuch G, Richter H, Voigt I, Noack M, Caro J. J Membr Sci. 2009; 329:11.

Europe PMC Funders Author Manuscripts

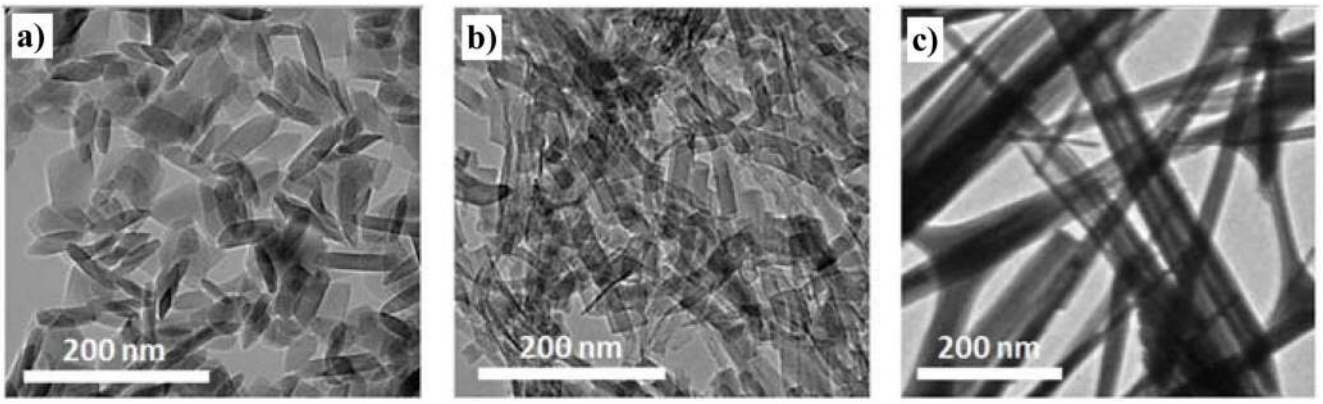

Figure 1.

TEM micrographs of a) NH_2-MIL-53(Al) nanoparticles, b) NH_2-MIL-53(Al) nanorods and c) NH_2-MIL-53(Al) microneedles. The dimensions of the particles can be found in Table 1.

Europe PMC Funders Author Manuscripts

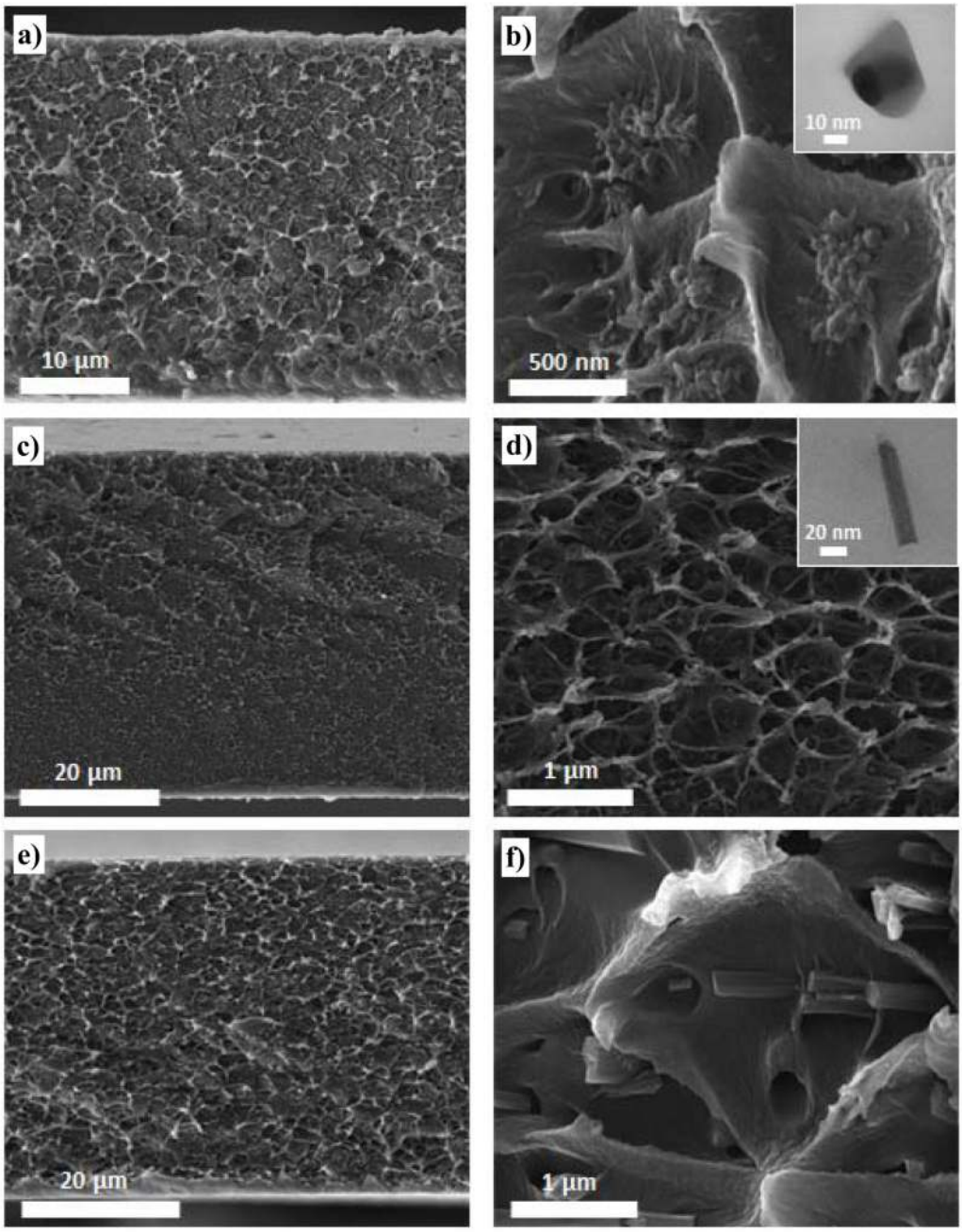

Figure 2.

SEM images of 8 wt% NH_2-MIL-53(Al)@Matrimid® MMMs synthesized using the three different crystal morphologies: a, b) nanoparticles (NP), c, d) nanorods (NR) and e, f) microneedles (MN). Inset: TEM micrographs of a particle embedded in Matrimid® acquired for the b) 8 wt% NP-NH_2-MIL-53(Al)@Matrimid® and d) 8 wt% NR-NH_2-MIL-53(Al)@Matrimid® MMMs.

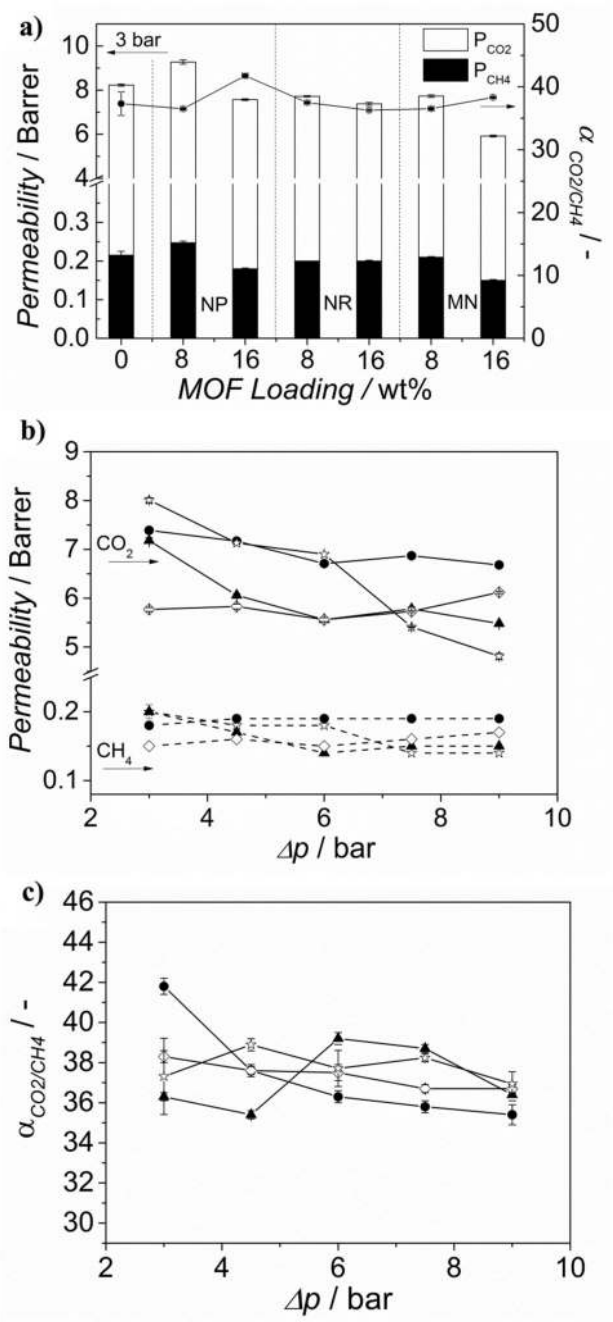

Figure 3.

a) Permeation properties for the CO_2/CH_4 mixture (1:1) separation at 298 K and $\Delta p = 3$ bar for MMMs comprising Matrimid® and NH_2 MIL 53(Al) MOF crystals with different morphologies (nanoparticles (NP), nanorods (NR) and microneedles (MN)) as a function of the filler loading. Effect of the trans-membrane pressure different on the b) CO_2 permeability and c) CO_2/CH_4 separation factor of the 16 wt% NH_2-MIL-53(Al)@Matrimid® MMMs prepared with different filler morphologies. The data are

average values of at least two membranes and error bars correspond to standard deviation. ▲ Nanorods, ● nanoparticles, ◊ microneedles and Matrimid®.

Europe PMC Funders Author Manuscripts

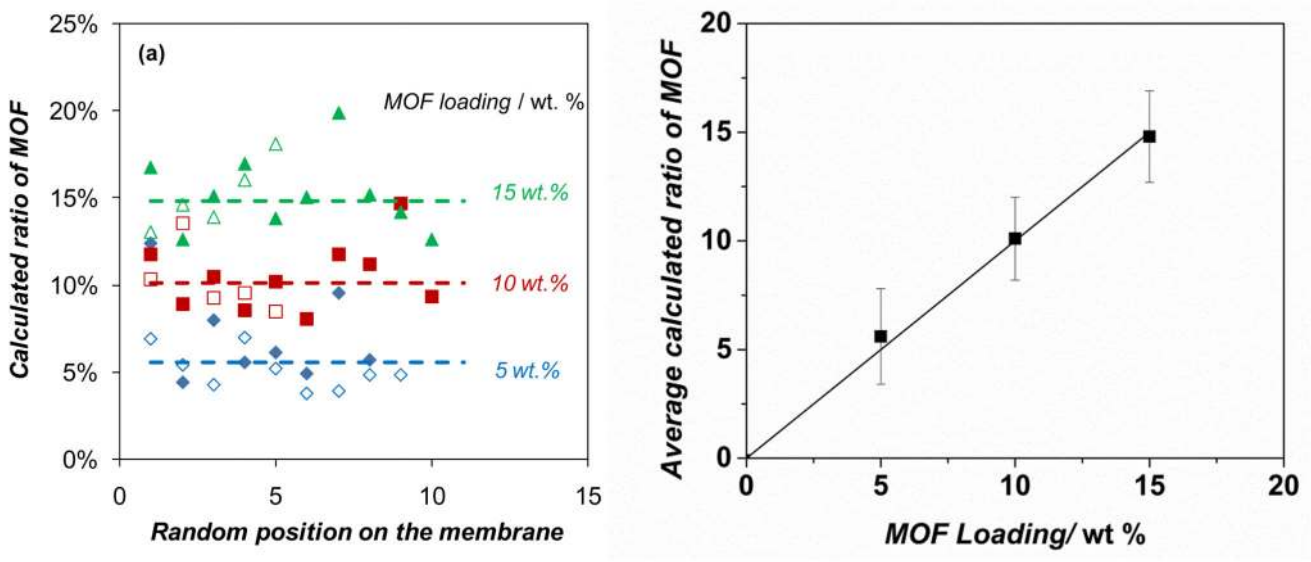

Figure 4.

Filler dispersion in the NH_2-MIL-53(Al)@6FDA-DAM MMMs evaluated by Raman spectroscopy. a) Contribution of NH_2-MIL-53(Al) in the modelled spectra at different locations on the membrane surface; b) comparison between the calculated spectroscopic ratio of NH_2-MIL-53(Al) and the nominal content in the membrane. In Figure a), full and empty symbols represent measurements on each side of the membrane; dotted lines show the average value for all measurements on each MMM.

Europe PMC Funders Author Manuscripts

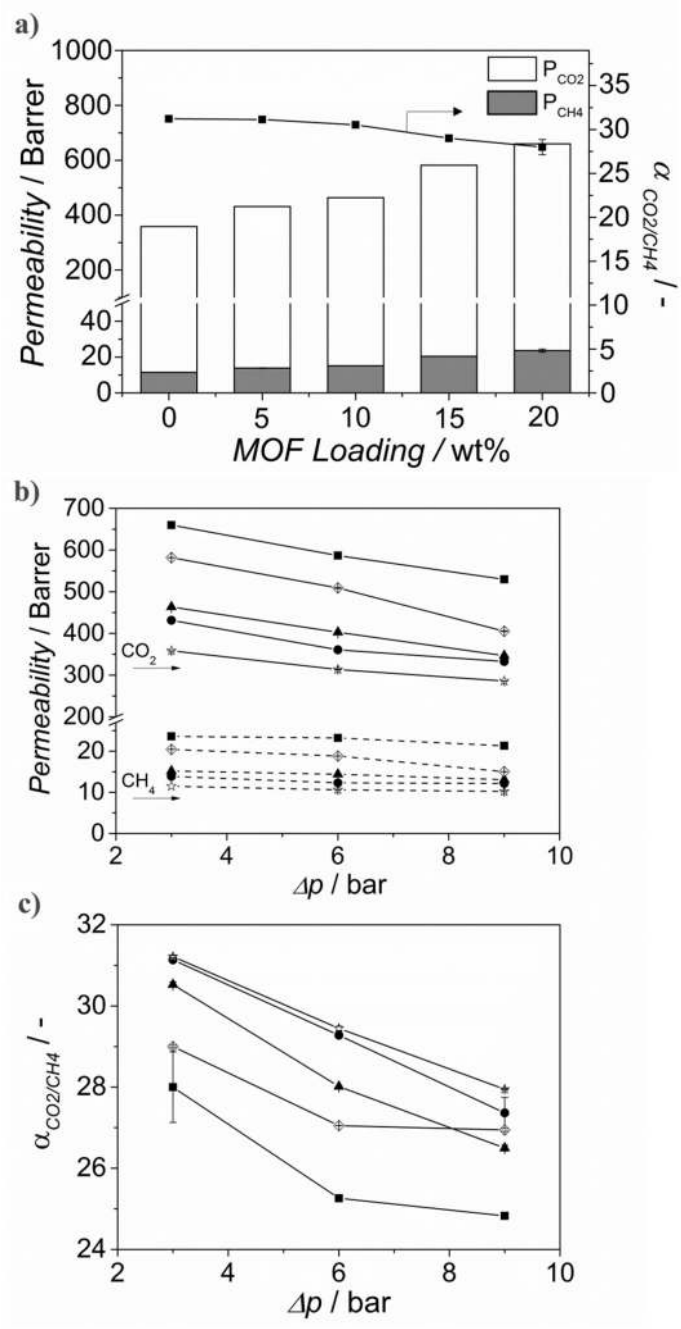

Figure 5.

a) CO_2 and CH_4 permeation properties measured for a 1:1 CO_2/CH_4 mixture at 298 K and Δp = 3 bar of MMMs comprising 6FDA-DAM and NH_2 MIL 53(Al) MOF nanoparticles as a function of the filler loading, influence of the trans-membrane pressure difference (Δp = 3, 6 and 9 bar), b) on the CO_2 permeability and c) on the selectivity of the NH_2 MIL 53(Al)@6FDA-DAM MMMs as a function of filler loading. The data are average values of at least two membranes and error bars correspond to standard deviation. ☆ bare 6FDA-

DAM and ● 5 wt%, ▲ 10 wt%, ◊ 15 wt% and ■ 20 wt% NH_2-MIL-53(Al)@6FDA-DAM MMMs, respectively.

Europe PMC Funders Author Manuscripts

Europe PMC Funders Author Manuscripts

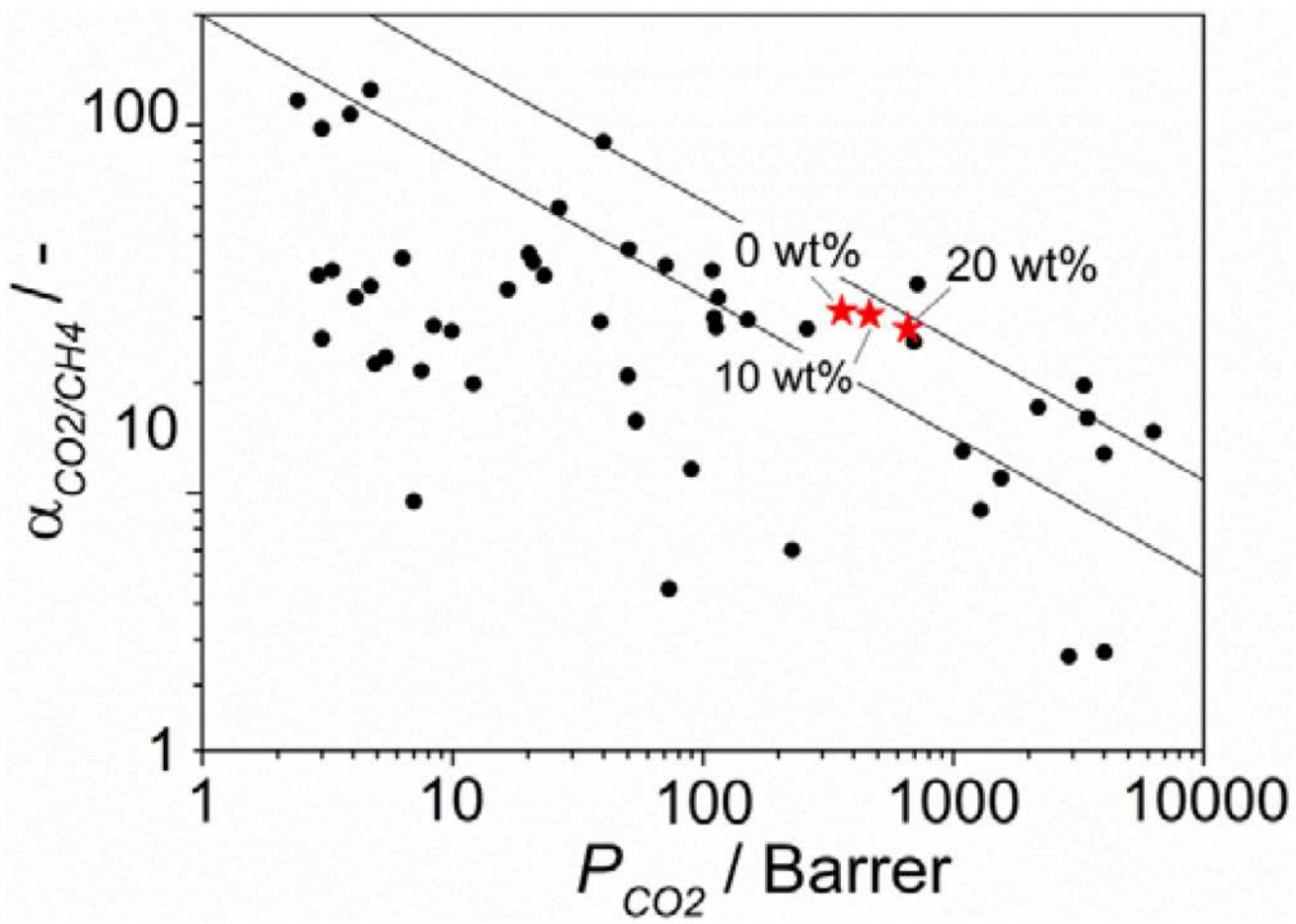

Figure 6.

Robeson plot for the separation of CO_2 from CH_4 showing the gas separation performance of pure 6FDA-DAM and of the MMMs prepared with 10 and 20 wt% of NH_2-MIL-53(Al) nanoparticles measured for a 1:1 CO_2/CH_4 mixture at 298 K and $\Delta p = 3$ bar. Most relevant results reported in literature for MOF-based MMMs have also been included for comparison.

Europe PMC Funders Author Manuscripts

Table 1

Dimensions of NH_2-MIL-53(Al) nanoparticles, nanorods and microneedles.

	Length	Width	Aspect ratio
Nanoparticles	46 ± 6 nm	15 ± 1 nm	3 ± 1
Nanorods	67 ± 14 nm	15 ± 3 nm	5 ± 1
Microneedles	4 ± 1 μm	80 ± 10 nm	48 ± 12